J. Space Weather Space Clim. 2017, 7, A27

DOI: 10.1051/swsc/2017025

SWSC

Available online at:
www.swsc-journal.org

RESEARCH ARTICLE OPEN ACCESS

Forecasting $E > 50$-MeV proton events with the proton prediction system (PPS)

Stephen W. Kahler[1,*], Stephen M. White[1] and Alan G. Ling[2]

[1] Space Vehicles Directorate, AFRL/RVBXS, Bldg 570, 3550 Aberdeen Dr. SE, Kirtland AFB, NM 87110, USA
[2] Atmospheric Environmental Research, 2201 Buena Vista Drive SE, Suite 407, Albuquerque, NM 87106, USA

Received 27 April 2017 / Accepted 6 September 2017

Abstract – Forecasting solar energetic ($E > 10$-MeV) particle (SEP) events is an important element of space weather. While several models have been developed for use in forecasting such events, satellite operations are particularly vulnerable to higher-energy (>50-MeV) SEP events. Here we validate one model, the proton prediction system (PPS), which extends to that energy range. We first develop a data base of $E > 50$-MeV proton events >1.0 proton flux units (pfu) events observed on the GOES satellite over the period 1986–2016. We modify the PPS to forecast proton events at the reduced level of 1 pfu and run PPS for four different solar input parameters: (1) all ≥M5 solar X-ray flares; (2) all >200 sfu 8800-MHz bursts with associated ≥M5 flares; (3) all >500 sfu 8800-MHz bursts; and (4) all >5000 sfu 8800-MHz bursts. The validation contingency tables and skill scores are calculated for all groups and used as a guide to use of the PPS. We plot the false alarms and missed events as functions of solar source longitude, and argue that the longitude-dependence employed by PPS does not match modern observations. Use of the radio fluxes as the PPS driver tends to result in too many false alarms at the 500 sfu threshold, and misses more events than the soft X-ray predictor at the 5000 sfu threshold.

1 Introduction

Accurate modeling and forecasting of solar energetic ($E > 10$-MeV) particle (SEP) events is important for a wide range of space operations (e.g., Crosby et al., 2015). It is well known that the largest SEP events are produced in shocks driven by fast (>800 km s^{-1}) coronal mass ejections (CMEs; e.g., Reames, 2013), so observations of CME properties are an obvious input source for SEP event forecast systems. CMEs typically follow associated solar X-ray flares in time and require longer observing timescales than flares to determine their characteristics, which presents an obstacle for acquiring CME measurements sufficiently prompt for timely SEP forecasts (St. Cyr et al., 2017). Solar flare X-ray and radio peak fluxes and fluences are available promptly and have also been found to provide reasonable bases for SEP event forecasts (Balch, 2008), and hence are used in many current forecasts.

Most statistical studies comparing SEP events with flares and CMEs are conducted for events with SEP energies of ≤25-MeV (Cane et al., 2010, Kahler, 2013). For practical applications to astronauts, communications, and satellite operations, it is recognized that the 50-MeV range is of greatest importance (Schwank et al., 2005, Posner, 2007, Tribble, 2010), although for specific applications such as single event upsets, lower ($E > 30$-MeV) energies are expected to be important (O'Brien, 2009). One forecast system, UMASEP, which matches derivatives of soft X-ray flare increases (Núñez, 2011) or microwave fluxes (Zucca et al., 2017) with initial increases of SEP intensities, has been extended to the 100-MeV range (Núñez, 2015). Two forecast systems, the proton prediction system (PPS), in current use by the 557th Air Squadron for the Air Force Weather Agency, and PROTONS, used by the Space Weather Prediction Center (SWPC) at the National Oceanic and Atmospheric Administration (NOAA; Balch, 1999, 2008) have options to forecast occurrence, peak intensities, and timings of 50-MeV proton events based on observed solar flares and radio bursts. The PROTONS forecast program is based on statistical analyses of prior data sets of SEP events and flares and uses a probability matrix of flare X-ray peak intensities and fluences to forecast the occurrence probability of an SEP event. It was validated[1] for $E > 10$-MeV proton events that occurred from 1986 to 2004 by Balch (2008). The PPS forecasts were validated for $E > 10$-MeV proton events that occurred from 1997 to 2001 by Kahler et al. (2007, hereafter KCL), but a systematic validation of 50-MeV forecasts with either model has not been carried out until now. This study responds to a request from the 557th Air Squadron to validate the PPS for 50-MeV proton event forecasts.

*Correspondence: stephen.kahler@us.af.mil

[1] Here we use "validate" in the sense common to forecasting studies, i.e., meaning "to measure forecasting performance".

The PPS takes as an input signal either an 0.05–0.4 or 0.1–0.8 nm soft X-ray observation from the GOES satellite, or a solar radio burst flux at one of several standard frequencies measured by the US Air Force Radio Solar Telescope Network (RSTN) system. The data can be supplied as a fluence or as a peak flux, and the solar flare position must also be specified. The PPS outputs consist of the beginning, peak, and end times, peak intensities I_p, and event fluences of 18 selected proton integral energy bands if the forecasted I_p reaches the 10 proton flux unit (pfu = 1 proton/cm^2 s sr) threshold established by SWPC as a level-1 radiation storm. The proton event beginning and end times refer to crossings of the threshold levels and define the time intervals of the fluences. The user selects the desired solar input variable and proton channel outputs. PPS is a science module of AF-GEOspace (Hilmer et al., 2012), a graphics-intensive software program combining space environment models, applications, and data visualization products developed by the Air Force Research Laboratory and the space weather community. Details of the PPS are described in the AF-GEO space user's manual version 2.5.1, which is publicly available at http://www.dtic.mil/dtic/tr/fulltext/u2/a563130.pdf.

The PPS model was introduced and reviewed in a series of works by Smart and Shea (1979, 1989, 1992) and briefly summarized by KCL. It assumes an instantaneous proton injection at the Sun at 0.25 h after the beginning of the associated X-ray/radio flare burst. The proton spatial injection profile in the corona is assumed to have a peak centered at the flare location and a gradient that imposes a correction of a factor of $\sim 10^{-\Theta}$, where Θ is the displacement in radians from the flare center (Shea et al., 1988). Scatter-free proton propagation is assumed with a 60° pitch angle in a uniform Parker spiral field with an Earth magnetic connection to W57.3° . The model calculates the time T_m of maximum intensity I_p using the expression

$$T_m(\text{hours}) = 8\Theta^2 + 2.0(0.13333D^2/\beta) \qquad (1)$$

where D is the distance along the Parker spiral in astronomical units (AU), and $\beta = v/c$ of the protons, where v is the proton speed. An exponential decay is assumed following the peak intensity. The peak proton intensities I_p are based on modifications to several models with X-ray and radio burst inputs, all of which were developed in the 1970s (Smart and Shea, 1979). Relatively few SEP events were well studied at that time, and the data sample available to derive the parameters for the model numbered of order 20 events (D. Smart, private communication). PPS calculates a value of I_p for all flares, but the operational version of PPS returns this value as a proton event forecast only if $I_p \geq 10$ pfu. We note that our inspection of the current PPS operating code reveals some modifications to the parametric values described above. In this work we use GOES 0.1–0.8 nm X-ray and RSTN radio burst inputs and focus on the PPS $E > 50$-MeV proton forecasts.

2 Data analysis

2.1 The $E > 50$-MeV proton event list

We first generated a list of all >1 pfu 50-MeV proton events observed with the Energetic Particle Sensors (EPS, Rodriguez et al., 2014) on the GOES satellites from 1986 to 2016. The $E > 50$-MeV proton quiet background is usually <0.05 pfu, so the 1 pfu threshold is ~20 × background and allows us to include in the PPS validation analysis those cases when a false alarm forecast was mitigated by the occurrence of an observed proton event with 1 pfu $< I_p <$ 10 pfu. The initial list, which included onset, peak and end times of all increases above 1 pfu, was inspected and corrected for two problems. First, we removed 20 cases of small (1.1–2.2 pfu) secondary maxima resulting from fluctuations below the 1 pfu threshold during the decay phases of earlier proton events. We then added the estimated times and I_p of 5 events which followed prior large >10 pfu events before the latter events decayed to the 1 pfu threshold. This yielded the peak intensities and times for a total of 138 $E > 50$-MeV proton events above the 1 pfu threshold. Of those, 71, which we call small proton events, had 1 pfu $< I_p <$ 10 pfu, and for 67 events $I_p \geq 10$ pfu. We note that Papaioannou et al. (2016) have recently generated a GOES-based list of proton events for four different integral energies. In the comparable energy range of $E > 60$-MeV and period 1984–2013, their list has a similar number of 72 small proton events but only 46 ≥ 10 pfu events; however, nearly all theirs have flare associations, while we retain all events independent of flare associations.

The goal of this application of the PPS program is to forecast only $E > 50$-MeV proton events of ≥10 pfu, so the subset of 67 observed ≥10 pfu events, listed in Table 1, are the basic forecast target against which we measure the performance of the PPS. The first three columns of Table 1 give the dates and times of SEP onsets, the peak intensities I_p in pfu, and the event fluences. Columns 4–7 give the start times of the associated X-ray flares, the peak fluxes in the CMX system, the rise times in minutes, and the flare longitudes. In three cases of high backgrounds the SEP event fluences could not be measured, and in 9 cases there was not a credible flare and/or source association, suggesting backside events. Two of the 67 events have associated flares <M5.

While we separately consider in our evaluations the nearly successful cases of PPS forecasts of proton events, which were followed by observed small proton events, we do not separately consider the few reverse cases in which PPS forecasts of small proton events were followed by the target proton events of ≥10 pfu intensities. Those forecasts are given in Table 1 but are treated statistically as missed events, along with observed proton events for which either no PPS forecast was run or the forecast was negative.

The PPS is designed to forecast a large fraction of observed proton events while minimizing the number of forecasted but unobserved (false alarm) events. The success of the PPS forecasts is evaluated with the standard Heidke (HSS) and true skill statistics (TSS) (e.g., see Woodcock, 1976;Wilks, 2011; Bloomfield et al., 2012). The HSS is a comparison with random forecasts with the same probabilities of forecasted and of observed events as in an assumed model. The TSS compares the outcome to an unbiased model in which the number of false alarms equals the number of missed events. For both HSS and TSS, a completely accurate forecast system yields a value of 1.0, one based on random chance gives 0, and a worse than random system gives negative values. The skill scores for each of the PPS forecast variables are given in Table 2, along with the FAR, the false alarm ratio, defined as the ratio of event

Table 1. The $E > 50$ MeV 10-pfu events, flare associations, and PPS outcomes.

SEP event			Flare event					PPS forecast (pfu)[b]	
SEP onset Date, time (UT)	Peak (pfu)	Fluence (p/cm^{-2})	Start Time[a]	Event Peak	Rise (min.)	Flare Long.	8800 (sfu)	X-ray Pred.	8800 Pred.
02/06/1986 09:35	15	1.01E+07	06:18	X1.7	7	W06	8800	–	26
03/11/1989 05:30	183	3.19E+06	18:48p	X4.5	24	E22	20 000	–	14
03/13/1989 05:25	10	4.37E+05	02:59	X1.2	21	W02	1400	–	(8)
03/17/1989 22:20	10	2.62E+06	17:29	X6.5	8	W60	7500	54	471
07/25/1989 09:00	18	5.32E+06	08:39	X2.6	4	W84	830	(2)	(7)
08/12/1989 16:00	557	4.77E+08	13:57	X2.6	27	W37	5900	38	606
09/29/1989 12:00	5650	9.59E+08	10:47	X9.8	46	W23	15 000	188	1110
10/19/1989 13:05	5150	2.25E+09	12:29	X13.0	26	E10	44 000	(8)	110
10/22/1989 18:00	700	–	17:08	X2.9	49	W31	39 000	70	5370
10/24/1989 18:00	500	–	17:36	X5.7	55	W57	48 000	643	24 100
11/15/1989 07:20	13	3.93E+06	06:38	X3.2	27	W26	3300	26	175
11/30/1989 17:25	42	2.99E+07	11:45	X2.6	40	W52	4400	127	1310
05/21/1990 22:55	62	2.33E+07	22:12	X5.5	5	W36	6400	11	114
05/24/1990 21:10	43	5.79E+07	20:46	X9.3	3	W78	45 000	10	459
03/23/1991 08:35	2510	4.87E+08	22:43p	X9.4	2	E28	37 000	–	–
05/13/1991 02:20	25	5.94E+06	01:03	M8.2	41	W90	190	(5)	11
06/04/1991 18:10	23	6.78E+07	03:37	X12	13	E70	33 000	–	–
06/11/1991 02:40	269	1.49E+08	02:09	X12	20	W17	17 000	54	358
06/15/1991 08:45	153	9.95E+07	06:33	X12	118	W69	17 000	2990	11 400
06/25/1992 20:25	37	1.51E+07	19:47	X3.9	24	W67	20 000	90	2950
10/30/1992 19:10	210	1.39E+08	17:02	X1.7	28	W61	9000	46	1920
11/02/1992 03:20	312	1.68E+08	02:31	X9.0	37	W90	17 000	115	995
09/03/1994 08:50	37	1.95E+05		None				NR	NR
09/04/1994 09:00	16	3.30E+05		None				NR	NR
09/05/1994 09:30	11	1.31E+05		None				NR	NR
09/06/1994 09:00	58	7.55E+05		None				NR	NR
11/06/1997 12:40	115	7.46E+07	11:49	X9.4	6	W63	10 000	54	424
04/20/1998 12:50	103	8.29E+07	09:38	M1.4	43	W90?		NR	NR
05/02/1998 14:00	24	8.38E+06	13:31	X1.1	11	W15	1700	–	16
05/06/1998 08:25	19	2.83E+06	07:58	X2.7	11	W65	2000	21	143
08/24/1998 23:10	11	1.08E+07	21:50	X1.0	22	E09	2100	–	(5)
09/30/1998 14:30	30	8.33E+06		None				NR	NR
11/14/1998 06:55	28	1.05E+07		None				NR	NR
07/14/2000 10:40	1670	1.37E+09	10:03	X5.7	21	W07	8900	(9)	86
11/08/2000 23:45	1880	1.16E+09	22:42	M7.4	46	W71	240	20	25
11/25/2000 20:00	19	7.48E+06	00:58	M8.2	32	E50	2800	–	–
04/03/2001 00:00	54	2.40E+07	21:32p	X20	19	W75	7600	386	591
04/15/2001 14:00	275	7.75E+07	13:19	X14.4	31	W85	1500	240	99
04/18/2001 02:45	40	1.86E+07		None		WL		NR	NR
08/16/2001 01:05	144	3.94E+07		None		bWL		NR	NR
09/24/2001 12:00	273	3.21E+08	09:32	X2.6	66	E23	23 000	–	35
10/01/2001 14:20	25	1.10E+07	04:41	M9.1	34	No L	130	NR	NR
11/04/2001 16:50	2120	9.87E+08	16:03	X1.0	17	W18	2400	(2)	53
11/22/2001 21:50	162	1.46E+08	22:32	M9.9	58	W36	790	28	166
12/26/2001 05:55	180	3.33E+07	04:32	M7.1	68	W54	3800	49	2060
04/21/2002 01:50	208	1.98E+08	00:43	X1.5	68	W84	2800	37	426
08/24/2002 01:30	76	1.87E+07	00:49	X3.1	23	W81	13 000	29	841
10/26/2003 18:10	10	3.03E+06	17:21	X1.2	58	W38	4500	40	1060
10/28/2003 11:40	1630	1.06E+09	09:51	X17.2	79	E08	70 000	57	658
11/02/2003 17:40	153	4.84E+07	17:03	X8.3	22	W56	17 000	308	3780
11/10/2004 03:10	13	4.83E+06	01:59	X2.5	14	W49	5000	27	459
01/16/2005 02:35	11	–	22:25p	X2.6	37	W05	21 000	(6)	305
01/17/2005 10:00	350	1.64E+08	06:59	X3.8	173	W25	16 000	357	5520
01/20/2005 06:50	1070	1.52E+08	06:36	X7.1	25	W61	62 000	266	12 100

Table 1. (continued).

SEP event			Flare event					PPS forecast (pfu)[b]	
SEP onset Date, time (UT)	Peak (pfu)	Fluence (p/cm^{-2})	Start Time[a]	Event Peak	Rise (min.)	Flare Long.	8800 (sfu)	X-ray Pred.	8800 Pred.
09/08/2005 01:20	50	8.14E+07	17:17p	X17.0	23	E77	23 000	–	–
12/06/2006 18:50	103	9.71E+07	18:29	X6.5	18	E64	13 000	–	–
12/13/2006 02:55	167	6.19E+07	02:14	X3.4	26	W23	7100	22	300
12/14/2006 22:50	11	2.37E+06	21:07	X1.5	52	W46	1900	98	1000
06/07/2011 07:10	14	7.92E+06	06:16	M2.5	25	W64	870		170
01/23/2012 04:45	76	6.61E+07	03:38	M8.7	21	W21	6900	(3)	201
01/27/2012 18:50	47	3.95E+07	17:37	X1.7	60	W71	810	83	241
03/07/2012 03:40	300	3.61+08	00:02	X5.4	22	E27	20 000	–	(6)
03/13/2012 17:55	24	4.44E+06	17:12	M7.9	29	W59	4100	19	965
05/17/2012 02:00	78	1.40E+07	01:25	M5.1	22	W76	630	(3)	52
05/22/2013 14:20	26	1.93E+07	13:08	M5.0	24	W70	83	(5)	–
01/06/2014 08:25	12	4.62E+06		None		bWL		NR	NR
01/07/2014 19:50	48	3.59E+07	18:04	X1.2	28	W11	1800	(2)	33

[a] p indicates preceding day.
[b] – indicates no ≥1 pfu PPS forecast; () indicates PPS forecast of 1–10 pfu; NR means the data available for the event are not sufficient to run PPS.

Table 2. PPS contingency table numbers and skill scores for various solar inputs.

Solar variable	Forecast	Observed[a]	Not observed	HSS[b]	TSS	POD	FAR
≥M5 X-ray flares	Yes	33 (+7)	64 (−7)	0.33	0.40	0.49	0.66
	No	34	603	(0.40)	(0.45)	(0.54)	(0.59)
8800-MHz bursts	Yes	44 (+27)	197 (−27)	0.16	0.34	0.66	0.82
With ≥M5 flares	No	23	417	(0.28)	(0.47)	(0.76)	(0.71)
All 8800-MHz bursts	Yes	44 (+22)	208(−22)	0.13	0.29	0.66	0.83
>500 sfu	No	23	356	(0.23)	(0.40)	(0.74)	(0.74)
All 8800-MHz bursts	Yes	27 (+7)	26 (−7)	−0.14	−0.15	0.40	0.49
>5000 sfu	No	40	21	(−0.01)	(−0.02)	(0.46)	(0.36)
KCL PPS >10-MeV	Yes	18	18	0.09	0.08	0.40	0.50
With ≥M5 flares	No	27	39	–	–	–	–

[a] Numbers in parentheses are additional PPS forecasts of >10 pfu observed as 1–10 pfu events but counted as Not Observed.
[b] Skill scores in parentheses calculated by moving the observed 1–10 pfu from "Not Observed" to "Observed".

forecasts that turn out wrong, and the POD, the probability of detection, also called the hit rate, defined as the fraction of events that were correctly forecasted (Wilks, 2011).

2.2 The solar flare X-ray and radio burst input groups

We test the PPS over the 1986–2016 period with four separate groups of solar flare event inputs. All flare inputs require solar flare locations: in the historical flare records, most locations are derived from simultaneous Hα observations which were not always available and could not see over-the-limb events. Accordingly, many events, including some of the largest, cannot be used in this validation due to the absence of locations.The first group used for validation are all 748 ≥M5 flares, and the second are the subset of those flares with RSTN solar 8800-MHz burst flux reports. For the third group we compiled a list from the RSTN observations of all 8800-MHz bursts with peak fluxes >500 solar flux units ($1\ \text{sfu} = 10^{22}\ \text{W m}^{-2}\ \text{Hz}^{-1}$), independent of associated X-ray bursts, and the fourth group are the subset of those bursts with fluxes >5000 sfu. The 8800-MHz frequency was chosen because it is usually close to the gyrosynchroton peak of typical radio bursts(Nita et al., 2002). The analysis consists of comparisons of the PPS forecasts with the observed $E > 50$-MeV events to determine numbers of correct event forecasts, false alarms, and missed events (observed event that was not forecast to occur). Note that the missed events fall into three groups: (i) those with no good flare candidates, such as over-the-limb events; (ii) those with <M5 flares as candidates, hence not matching our X-ray sample; and (iii) those events in our samples for which PPS forecast an I_p value that did not exceed the threshold. Since the purpose of this validation is to forecast 50 MeV events, we use the full list of such events even

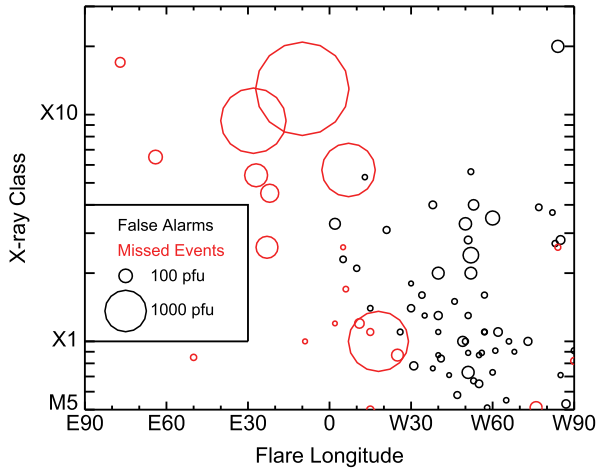

Fig. 1. Longitude plot of the PPS 22 missed proton events (red circles) and 64 false alarms (black circles) as a function of the associated flare X-ray peak flux. Circle diameters scale with I_p of missed observed (red) or false forecasts (black).

though we know in advance that some of them cannot be correctly forecasted by our data samples. We discuss the flare selections and PPS results in the following sections.

2.3 The ≥M5 X-ray flares

The PPS program has two options for 0.1–0.8 nm X-ray flare inputs, the peak fluxes and the fluences. Recent studies have shown that X-ray fluences give better correlations with proton intensities I_p than do peak fluxes (KCL; Balch, 2008), so here we use fluence as the input variable. PPS allows two alternative sets of inputs to specify the fluence: one can choose to use the GOES peak 0.1–0.8 nm flux, FXW (ergs cm^{-2} s^{-1}), together with the X-ray flare rise time from onset to peak, ΔT (minutes), in which case PPS scales the product FXW × ΔT to a fluence; or one can supply FX, the actual X-ray flare fluence calculated from flare onset to the half-power decay time. Balch (2008) used the latter version along with a flare threshold of >C2.5 to validate PROTONS, but that form of fluence is not readily tabulated for events in the early years of this study. In this work, following KCL, we choose the former method for providing the fluence, and impose a threshold peak flux of GOES M5 to define our sample. We used the GOES X-ray flare lists from the NOAA National Geophysical Data Center (NGDC) site at https://www.ngdc.noaa.gov/stp/space-weather/solar-data/solar-features/solar-flares/x-rays/goes/xrs/ to compile our list of 748 ≥ M5 flares over the period 1986–2016. Thirty two of the 748 flares had no associated flare locations, reducing the total to 716 candidate flares. PPS did not run for 17 of the flares with locations, all occurring before 1993, because the onset and peak times given in the flare lists were identical. The resulting zero rise times yielded zero fluences with our approach. For those events we replaced the listed times with appropriate values based on other records. In all 17 cases PPS did not forecast a > 1 pfu proton event, and they are included in the 620 correctly forecasted null events.

The PPS ≥ M5 flare results are shown in the first part of Table 2, where we separately call out the 7 cases of false alarms for which a > 1 pfu proton event was observed. If one counts those cases as successful forecasts rather than false alarms, then we would have 40 correct forecasts and 57 false alarms. We also give in Table 2 Heidke (HSS) and true skill scores (TSS) for the forecast contingency table. Among the 34 missed events one did not have a flare location (an M9 on 2 October 2001) and another 11 did not have associated ≥M5 flares, so PPS was not run for those 12 cases. The 64 false alarms included two forecasts of modest proton events to occur on 3 November 2003 during the decay of a large proton event of the previous day. We cannot exclude the possibility of correct proton forecasts for those two cases, but we treat them as false alarms.

It is of interest to look for trends in the solar longitudes of the 64 false alarms and 22 missed events with known source longitudes. Figure 1 shows a longitude plot of peak X-ray flare fluxes of the false alarms and missed events, with the data circles scaled to the I_p values. There is a clear trend for over-prediction with well connected (W30°–W70°) flares and an under-prediction for eastern hemisphere flares, several of which had very large X-ray flares and proton events. Of the 57 false alarms with no observed event of any size, the median forecast of I_p was only 18 pfu. The two false alarms with highest forecast I_p were 24 June 1988 at 135 pfu and 14 August 1989 at 108 pfu. Their associated flares were an X2.4 flare at W52° and an X3.5 at W60°, respectively.

We examine three egregious cases of missed events. The first event, of 19 October 1989, had an observed >50-MeV I_p of 5150 pfu and was associated with an X13 flare at E10°. PPS forecasted a SEP event with I_p = 7.5 pfu, slightly below the 10 pfu threshold required for a hit, but nearly three orders of magnitude below the observed value. The second event, of 23 March 1991, with an observed I_p = 2510 pfu was associated with an X9 flare 22 March at E28°. PPS forecast neither a > 50-MeV event above 1 pfu nor a > 10-MeV event above 10 pfu and may have been undermined by the short 2-min X-ray rise time used in the X-ray fluence input calculation. The third event, on 4 November 2001, had an observed I_p = 2120 pfu,and was associated with an X1 flare at W18°. Similar to the first event, PPS forecast I_p = 1.7 pfu, below the 10 pfu threshold and three orders of magnitude below the observed peak.

The PPS forecasts include both I_p and fluences (above 10 pfu) of SEP events. In the left side of Figure 2 we compare the forecasted versus observed I_p of the 33 correctly forecasted events and the 7 additional events for which a PPS forecast matched an observed SEP event of 1 to 10 pfu. The correlation coefficient is CC = 0.29 for those 40 events. We reset the PPS outputs to calculate the event fluences above 1 pfu and compare those with the matching values calculated from the GOES profiles. Since we added two events for which the prior backgrounds were not below 1 pfu and we could not calculate separate fluences, we have a total of 38 events, shown in Figure 3. The CC = 0.22 for those events.

2.4 The 8800-MHz bursts with ≥M5 X-ray flares

From our first list of 748 ≥ M5 X-ray flares we selected a subset of 657 flares with reported 8800-MHz bursts with peak fluxes >200 sfu to run the PPS with radio burst inputs. The

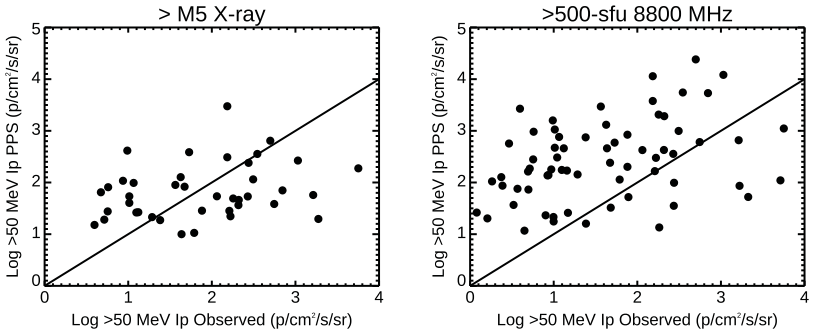

Fig. 2. Left: Plot of the PPS forecasted versus observed >50-MeV I_p for 33 correctly forecasted events and the 7 forecasted false alarms with observed I_p between 1 and 10 pfu. The PPS was run with flare X-ray inputs. Right: Same for the 44 correctly forecasted events and 22 forecasted events with observed I_p between 1 and 10 pfu, with PPS run for the >500 sfu 8800-MHz bursts. Diagonal lines in each plot correspond to correct forecasts.

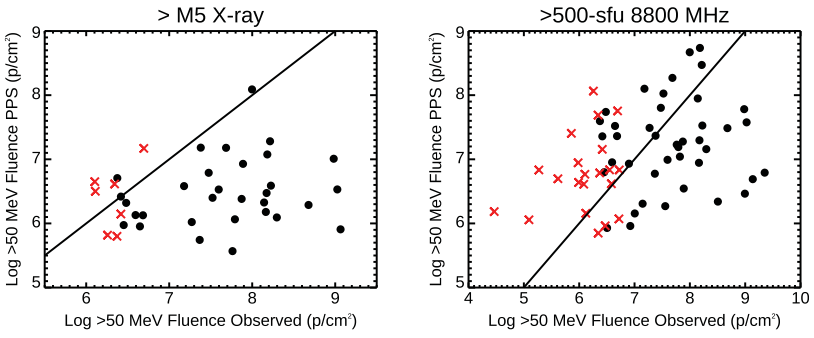

Fig. 3. Left: Plot of the PPS forecasted versus observed >50-MeV fluences above 1 pfu for events with $I_p > 1$ pfu. Red crosses are the 7 PPS false alarms with observed $I_p > 1$ pfu. The PPS was run with flare X-ray inputs. Right: Same for the PPS forecasted events run with >500 sfu bursts. Diagonal lines in each plot correspond to correct forecasts.

8800-MHz burst fluxes were extracted from the lists of fixed-frequency bursts maintained by NGDC at ftp://ftp.ngdc.noaa.gov/STP/space-weather/solar-data/solar-features/solar-radio/radio-bursts/reports/fixed-frequency-listings/. These lists cover the years 1960–2010; for the years 2011–2016, 8800-MHz burst fluxes were extracted from the reports in the daily solar event files issued by SWPC. Where multiple reports were provided for the same flare, the larger peak flux was generally used (except in a few cases where a report was clearly erroneous). The question here is whether using a double threshold for both X-ray flare and radio peak will improve the forecasts. The median 8800-MHz burst was 905 sfu, and the forecast contingency table is given on the second tier of Table 2. With these 8800-MHz burst inputs, 44 of the 67 > 50-MeV proton events were correctly forecasted, but there were now 197 false forecasts, including 27 events with observed peak intensities of >1 pfu. The skill scores of the table indicate that PPS performs somewhat worse by over-forecasting proton events with these radio burst inputs than with the X-ray fluence inputs.

2.5 All 8800 MHz bursts >500 sfu

The previous two groups required the occurrence of an ≥M5 flare with a known location. We now focus solely on the radio burst inputs to PPS and start with a selection of all large 8800 MHz bursts with peak fluxes of >500 sfu and known longitude sources, but with no requirement for X-ray flare associations. As for the X-ray validation, we use radio bursts occurring in the period 1986–2016. Of 694 total bursts, 612 had known solar locations and were used to generate PPS forecasts. The results are shown on the third tier of Table 2, and are broadly similar to the radio predictions for the ≥M5-selected sample. As with the ≥M5 flares, we show the corresponding longitude plot of missed events and false alarms for the >500 sfu bursts in Figure 4. We show the matching PPS versus observed peak fluxes and fluences on the right sides of Figures 2 and 3.

2.6 All 8800-MHz bursts >5000 sfu

A common feature of the two sets of forecasts based on radio burst fluxes discussed above is the large number of false alarms. The question arises as to whether there is a flux threshold that reduces the number of false-alarm forecasts while maintaining successful correct forecasts. To test this idea we selected from the previous group of 8800-MHz bursts only those with peak fluxes of >5000 sfu. There were only 90 such bursts, of which 9 did not have known source locations, leaving a total of 81 PPS runs. The resulting change from the previous larger group is to drive down substantially the false-alarm numbers (from 208 to 26) but at the cost of allowing the

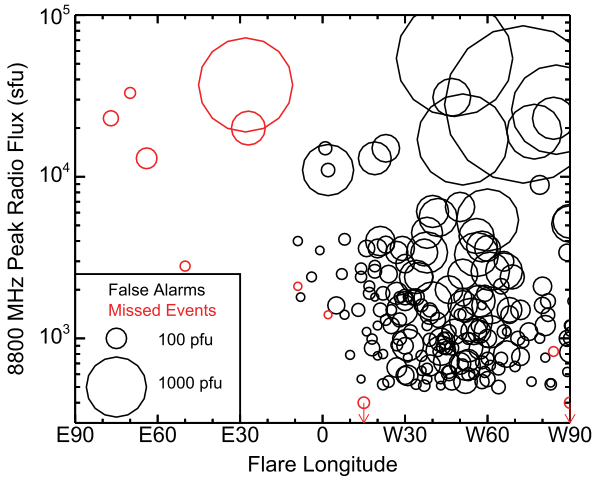

Fig. 4. Longitude plot of the PPS 11 missed proton events (red circles) and 186 false alarms (black circles) as a function of the associated >500 sfu 8800-MHz peak burst. Circle diameters scale with the I_p of missed observed (red) or false forecasts (black), as in Figure 1. The two red arrows indicate missed events for which the peak 8800-MHz burst was <300 sfu.

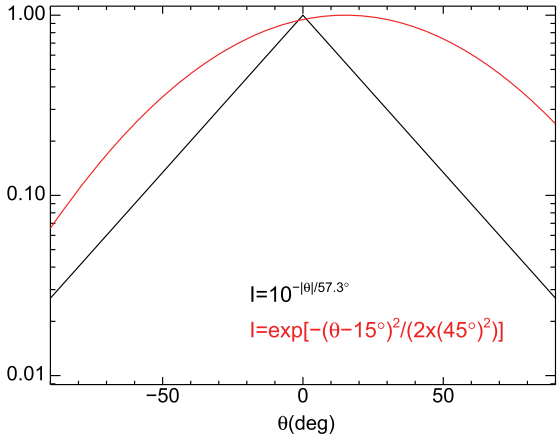

Fig. 5. Comparison of model SEP injection profiles I_p versus solar longitude, where $\theta = 0$ is the assumed location of the associated flare. Black profile is the PPS assumed gradient of a factor of 10 per radian, and the red profile is the approximate Gaussian fit assumed from multi-spacecraft observations of SEP events by Lario et al. (2013). The Gaussian profile is offset about 15° west of the flare longitude.

missed events to rise significantly (from 23 to 43). Note that now the incorrect forecasts of false alarms (26) and missed events (40) exceed the correct forecasts of hits (27) and nulls (21), producing negative skill scores, which tells us that such forecasts are worse than random chance.

3 Discussion

The goal of this work is to validate the PPS for $E >$ 50-MeV proton events. We have used the largest available data base of reported X-ray flares and energetic proton events, from 1986 to 2016, to generate an optimum statistical basis for the validation. The number of $E > 50$-MeV proton events in that period was only 67, so we enhanced the comparison between forecasted and observed events by including another 71 small ($1 < I_p < 10$ pfu) proton events over the same time interval. The first two lines of Table 2 show skill scores of ≈0.40 for PPS forecasts of ≥10 pfu proton events when using X-ray flares (observed in real time with the GOES satellites) as the primary input.

We asked whether flare microwave (8800-MHz) bursts produce better forecast results than the X-ray flares as PPS inputs. In the cases of microwave bursts with and without associated ≥M5 X-ray flares the event forecasts were worse, as the false alarm rates increased much more than the missed event rates decreased (Table 2). Selecting only the very largest 8800 MHz bursts produced the surprising results of negative skill scores, suggesting little if any physical coupling between those bursts and the $E > 50$-MeV proton events.

We further compared the X-ray and microwave-burst PPS forecasts of event I_p and fluences, shown in Figures 2 and 3. The X-ray forecasts of I_p generally lie along the line of correct values in Figure 2, but the 8800-MHz bursts give forecasts of values predominately exceeding that line, so for I_p values the X-ray forecasts are superior. On the other hand, if event fluences are the more important parameter for forecast applications, then Figure 3 shows that the 8800-MHz bursts give a better result since the PPS under-forecasts the fluences when used with the X-ray inputs. This comparison is based on observed and forecasted event fluences above 1 pfu, which may be somewhat different from results based on a 10 pfu threshold.

Having done PPS validations for $E > 50$-MeV proton events, we can compare our results with those of KCL for $E > 10$-MeV proton events, which were limited to only 78 PPS runs with ≥M5 flares during the 5-year period 1997–2001. We first modified their reported number of 3 events missed after running PPS by adding back the 24 observed proton events for which PPS was not run. That combined number is then comparable to our combined numbers of missed events for $E > 50$-MeV. The results are shown as the last entry in Table 2, where it is very clear from their low skill scores that PPS gave results for the >10-MeV events far inferior to those obtained here for >50-MeV events.

It is important to understand the input conditions when PPS yields more or less successful forecast outcomes. We selected solar longitude as an organizing parameter and show the missed-event and false-alarm results for the ≥M5 flares and >500 sfu bursts in Figures 1 and 4. There is a tendency for missed events to lie in the east and false alarms in the west, suggesting an overestimation in the PPS of the longitudinal gradient of the SEP source regions at the Sun. The proton-event longitudinal gradients were poorly known when the PPS was designed in the 1980s, but recent studies have refined our knowledge of those gradients, particularly with the help of multiple spacecraft observations of individual events (Lario et al., 2013, 2014). In Figure 5 we compare the longitudinal profile of proton intensities I_p used in the PPS with that typical of recent observational studies. The primary difference is the broader longitudinal extent of the assumed Gaussian fits to the observed events, which might qualitatively explain why the PPS over-forecasts proton events close to the solar flare longitudes and under-forecasts those further away. However, for the three large missed SEP events discussed in Section 2.3,

the model I_p values of Figure 5 are lower than the observational fit by less than a factor of 3, while the PPS produced values of I_p about three orders of magnitude too small. Those SEP events may have been outliers in the general correlation between flare X-ray fluences and SEP peaks, but the PPS failed to forecast any SEP event east of E23° for the 8800 MHz bursts or east of E08° for the X-ray flares. A flare at E20° corresponds to $\Theta = -77°$ in Figure 5, where the PPS gradient value is diminished by a factor of only about 25 from that of the peak at 0°. This would not seem to preclude PPS forecasts of SEP events east of about E20°, so we have no explanation for the lack of forecasted eastern SEP events.

The center of the false-alarm longitudinal distribution of Figure 1 also appears shifted somewhat to the east of W57° , perhaps consistent with the ~15° westward shift from W57° of the observational Gaussian fit. The observed westward shift has been explained by Lario et al. (2014) in terms of an assumed maximum acceleration of protons at the shock nose, which begins only after the nose is well above the flare site but is then magnetically connected to a site west of the flare.

Longitudinal dependence is also a fundamental difference between the PPS and PROTONS (Balch, 2008) forecasts of proton I_p. Balch (1999) considered applying a correction for longitudinal position in predicting I_p, but concluded that it made the predictions worse. The forecast of I_p from the current operational version of PROTONS is independent of longitude, while PPS assumes the exponential gradient shown in Figure 5. In our 50-MeV proton validation of PPS the positive CC of 0.29 for I_p (Fig. 2) and 0.22 for the event fluences (Fig. 3) would suggest that the longitudes should be included in the I_p forecasts. Looking back at the $E > 10$-MeV proton validations of PROTONS (Balch, 2008) and PPS (KCL), we find that in both studies the CCs of forecasted and observed I_p were quite similar (0.52 for 127 events (PROTONS) and 0.55 for 78 events (PPS)). While KCL used only a subset of the events of Balch (2008), this comparison suggests that while a longitudinal dependence of I_p is present, it is a secondary factor compared to the dependence on the flare X-ray fluence.

We have noted the limited comparison between the $E >$ 10-MeV and $E > 50$-MeV forecasts of the PPS. A useful exercise for the future might be to validate the PPS as a function of energy over a common data set of proton events and then to do inter-comparisons with forecasts of PROTONS or other models.

4 Conclusions

The PPS forecasting system, in use today but based on limited SEP data sets available several decades ago, has been tested against a comprehensive set of 67 $E > 50$-MeV proton events from 1986 to 2016. We tested four different sets of X-ray flare and radio burst inputs and evaluated each set with standard skill scores. The ≥M5 flare set gave results superior to those based on the 8800-MHz radio bursts. As the 8800-MHz burst test thresholds increased, the results, shown in Table 2, became dramatically worse. Within the limitations of the PPS model the X-ray flares, besides being the most immediately obtainable parameters, provide the best results. There is a clear longitudinal bias for missed events to lie in the eastern hemisphere and for false alarms in the western hemisphere (Figs. 1 and 4), but the assumed PPS longitudinal gradient is not significantly different from recent observational intensity profiles (Fig. 5). The X-ray flare inputs produced better I_p (Fig. 2) but worse fluence (Fig. 3) forecasts than did the 8800-MHz bursts.

Acknowledgments. S. Kahler was funded by AFOSR Task 15RVCOR167. A. Ling was supported by AFRL contract FA9453-12-C-0231. All data for this paper is properly cited and referred to in the reference list. The editor thanks two anonymous referees for their assistance in evaluating this paper.

References

Balch CC. 1999. SEP proton prediction model: verification and analysis. *Radiat Meas* **30**: 231–50

Balch CC. 2008. Updated verification of the Space Weather Prediction Centers solar energetic particle prediction model. *Space Weather* **6**: S01001. DOI: 10.1029/2007SW000337.

Bloomfield DS, Higgins PA, McAteer RTJ, Gallagher PT. 2012. Toward reliable benchmarking of solar flare forecasting methods. *Astrophys J Lett* **747**: L41. DOI: 10.1088/2041-8205/747/2/L41.

Cane HV, Richardson IG, von Rosenvinge T. 2010. A study of solar energetic particle events of 1997-2006: their composition and associations. *J Geophys Res* **115**: A08101. DOI: 10.1029/2009JA014848.

Crosby N, et al. 2015. SEPEM: a tool for statistical modeling the solar energetic particle environment. *Space Weather* **13**: 406–26. DOI: 10.1002/2013SW001008.

Hilmer RV, Hall T, Roth C, Ling AG, Ginet GP, Madden D. 2012. AF-GEOSPACE user's manual version 2.5.1 and version 2.5.1P. AFRL Tech. Rep. AFRL-RV-PS-TR-2012-0143, p. 116

Kahler SW. 2013. A comparison of solar energetic particle event timescales with properties of associated coronal mass ejections. *Astrophys J* **769**: 110. DOI: 10.1088/0004-637X/769/2/110.

Kahler SW, Cliver EW, Ling AG. 2007. Validating the proton prediction system (PPS). *J Atmos Solar-Terr Phys* **69**: 43–9. DOI: 10.1016/j.jastp.2006.06.009.

Lario D, Aran A, Gómez-Herrero R, Dresing N, Heber B, Ho GC, Decker RB, Roelof EC. 2013. Longitudinal and radial dependence of solar energetic particle peak intensities: STEREO, ACE, SOHO, GOES, and MESSENGER Observations. *Astrophys J* **767**: 41. DOI: 10.1088/0004-637X/767/1/41.

Lario D, Roelof EC, Decker RB. 2014. Longitudinal dependence of SEP peak intensities as evidence of CME-driven shock particle acceleration. In: Hu Q, Zank GP, eds. Outstanding problems in heliophysics: from coronal heating to the edge of the heliosphere. ASP Conference Series, Vol. 484, pp. 98–103.

Nita GM, Gary DE, Lanzerotti LJ, Thomson DJ. 2002. The peak fluxdistribution of solar radio bursts. *Astrophys J* **570**: 423–438. DOI: 10.1086/339577.

Núñez M. 2011. Predicting solar energetic particle events (E >10MeV). *Space Weather* **9**: S07003. DOI: 10.1029/2010SW000640.

Núñez M. 2015. Real-time prediction of the occurrence and intensity of the first hours of >100 MeV solar energetic proton events. *Space Weather* **13**: 807–19. DOI: 10.1002/2015SW001256.

Papaioannou A, Sandberg I, Anastasiadis A, Kouloumvakos A, Georgoulis MK, Tziotziou K, Tsiropoula G, Jiggens P, Hilgers A. 2016. Solar flares, coronal mass ejections and solar energetic particle event characteristics. *J Space Weather Space Clim* **6**: A42. DOI: 10.1086/339577.

O'Brien TP. 2009. SEAES-GEO: a spacecraft environmental anomalies expert system for geosynchronous orbit. *Space Weather* **7**: 09003. DOI: 10.1029/2009SW000473.

Posner A. 2007. Up to 1-hour forecasting of radiation hazards from solar energetic ion events with relativistic electrons. *Space Weather* **5**: S05001. DOI: 10.1029/2006SW000268.

Reames DV. 2013. The two sources of solar energetic particles. *Space Sci Rev* **175**: 53–92. DOI: 10.1007/s11214-013-9958-9.

Rodriguez JV, Krosschell JC, Green JC. 2014. Intercalibration of GOES 8-15 solar proton detectors. *Space Weather* **12**: 92–109. DOI: 10.1002/2013SW000996.

Schwank JR, et al. 2005. Effects of particle energy on proton-induced single-event latchup. *IEEE Trans Nucl Sci* **52**: 2622–9. DOI: 10.1109/TNS.2005.860672.

Shea MA, Smart DF, Adams JH Jr, Chenette D, Feynman J, Hamilton DC,Heckman GR, Konradi A, Lee MA, Nachtwey DS. 1988. Toward a descriptive model of solar particles in the heliosphere. In: Feynman J, Gabriel S, eds. Proc. Interplanetary Particle Environment Conf. JPL Publ. 88-28. Pasadena, CA: JPL, p. 3

Smart DF, Shea MA. 1979. PPS76: a computerized event mode solar proton forecasting technique. In: NOAA Solar-Terrest. Predictions Proc., Vol. 1, pp. 406–427

Smart DF, Shea MA. 1989. PPS-87 – a new event oriented solar proton prediction model. *Adv Space Res* **9**: 281–4. DOI: 10.1016/0273-1177(89)90450-X.

Smart DF, Shea MA. 1992. Modeling the time-intensity profile of solar flare generated particle fluxes in the inner heliosphere. *Adv Space Res* **12**: 303–12. DOI: 10.1016/0273-1177(92)90120-M.

St. Cyr OC, Posner A, Burkepile JT. 2017. Solar energetic particle warnings from a coronagraph. *Space Weather* **15**: 240–57. DOI: 10.1002/2016SW001545.

Tribble A. 2010. Energetic particles and technology. In: Schrijver CJ, Siscoe GL, eds. Heliophysics: space storms and radiation: causes and effects. London: Cambridge Univ. Press, pp. 381–399.

Wilks DS. 2011. Statistical methods in the atmospheric sciences. Internat. Geophys. Ser., 100. Boston: Elsevier.

Woodcock F. 1976. The evaluation of yes/no forecasts for scientific and administrative purposes. *Month Weather Rev* **104**: 1209. DOI: 10.1175/1520-0493(1976)104 <1209:TEOYFF >2.0.CO;2.

Zucca P, Nez M, Klein K-L. 2017. Exploring the potential of microwave diagnostics in SEP forecasting: the occurrence of SEP events. *J Space Weather Space Clim* **7**: A13. DOI: 10.1051/swsc/2017011.

Cite this article as: Kahler SW, White SM, Ling AG. 2017. Forecasting $E > 50$-MeV proton events with the proton prediction system (PPS). *J. Space Weather Space Clim.* **7**: A27